MECHANISM OF CORROSION OF STEEL STRANDS IN POST TENSIONED GROUTED ASSEMBLIES

Alberto Sagüés[*], Rodney G. Powers[+], Hongbin Wang[*]
[*]Department of Civil and Environmental Engineering, University of South Florida
4202 East Fowler Ave. Tampa, FL 33620

[+]Florida Dept. of Transportation, Material Office
2006 NE Waldo Rd, Gainesville, FL 32609

ABSTRACT

In this preliminary study, the complexity of the corrosion phenomenon of post-tensioning strands in grouted anchorage assemblies was examined and both physicochemical and electrochemical key technical issues were identified. Measurements of oxygen reduction efficiency in high pH electrolytes were conducted to obtain polarization parameters to be used in modeling. The time evolution of electrical resistivity of 5 low-bleed commercial grouts was measured also for model input. A mathematical model for a simple grout-strand system was proposed and dimensionless equations were formulated, to solve the combined polarization and oxygen transport problem. Within the range of validity of the model assumptions, initial computations indicated that oxygen availability was a key factor in determining corrosion severity while grout resistivity was secondary. Predicted corrosion rates were in general agreement with field and laboratory observations. Issues for subsequent model development were identified.

Keywords: post-tensioning, strand, grout, anchorage, oxygen diffusivity, resistivity

INTRODUCTION

In post-tensioning (PT) of concrete a compressive force is applied by stressing tendons (or bars) after the concrete is cast and cured so that deflection and cracking are minimal, even at full load. Severe corrosion distress and even complete failure of external PT was recently observed in tendons of pillars or superstructure of three Florida pre-cast segmental bridges over salt water. As PT tendons are critical to the integrity of these structures, the investigation described here was initiated to investigate the corrosion mechanism.

Nature of the problem: The first reported incident was at the 18-year old Niles Channel Bridge in the Florida Keys (Powers, 1999, Sagüés, 2000) followed by the 7-year old Mid Bay Bridge (MBB) in the Western panhandle (Corven, 2001) and the 15-year old Sunshine Skyway Bridge over Tampa Bay (FDOT, 2002). In those structures, the tendons are a bundle of typically 19 or more seven-wire high-strength (ultimate tensile strength 1.86 GPa (270 ksi)) steel strands, contained for much of the length (including the part of the tendon that is external to the concrete) in a high-density polyethylene (HDPE) duct. The tendon terminates at anchorage assemblies (Figure 1) that transfer the longitudinal tendon force to the concrete. Portions of the tendon pass through pipes in intermediate deviation blocks or U-bends to provide lateral force transfer where needed. After tensioning the entire space between tendon and ducts or anchorage is pumped full with a cementitious grout. The grout is intended for corrosion protection of the steel by providing a highly alkaline environment, and also to allow for some force transfer between strand and anchorage in case of strand breakage or loosening.

The observed damage consisted, in each of the three bridges, of one completely separated tendon plus one to several partially detensioned tendons. The completely separated tendons had failed in the anchorage region following severe corrosion of many of the strands, as illustrated in Figure 2. Mechanical failure appears to be the result of simple overload due to locally reduced cross-section, usually in the form of generalized corrosion along several cm with occasional pitting.   In the partially detensioned tendons severe corrosion and mechanical failure had affected some but not all of the strands. In one instance the area of severe corrosion was about 2-3 m away from the anchorage. All cases of severe corrosion were associated with large void areas that should have been filled with grout. Significant chloride contamination of the remaining grout was observed at the corroded regions. In nearly all cases the affected anchorages were at bridge expansion joints, or underneath horizontal surfaces, where salt and moisture availability was significant. Additionally, HDPE duct cracks were commonly encountered in MBB. Corrosion was not unique to any particular anchorage manufacturer.

The available evidence suggests that the key deterioration factor was the formation of large grout voids at or near the anchorages. The most likely cause of voids is the development of large amounts of bleeding water during the grouting process of the materials used for grouting at the time of construction of the affected bridges (Ghorbanpoor, 1993, Powers, 2001). Bleeding is assisted by wicking of water along the strands and vibration resulting from the grout pumping operations. The bleed water may be subsequently reabsorbed into the grout or lost by evaporation through incomplete anchorage sealing that may result from deficiencies at the pour back on the wedge plate, or elsewhere (e.g. duct connections or duct cracking). Thus, some of the steel is not in contact with the protective highly alkaline grout that is intended to promote passivity of the steel surface. The region where the steel emerges from the grout-void interface may be particularly vulnerable because of a combination of detrimental factors. The pH of the grout pore water there could be lowered by carbonation from atmospheric carbon dioxide. At the same time evaporative local chloride ion enrichment may occur, elevating the chloride content (that could be either the small native content of the grout or some larger amount from external contamination) to a level sufficient to cause passivity breakdown at the local pH and potential conditions (Li, 2001, Moreno, 1998). After corrosion initiation there, aggravation may result from galvanic coupling of the

relatively small active region with a larger passive surface consisting of the rest of the strand assembly in the grout, plus other metallic regions of the anchorage. In the absence of free bleed water, the extent of the corrosion macrocell action is expected to depend on the polarization characteristics of the anodic and cathodic zones involved, and on the resistivity of the intervening hardened grout. The corrosion scenario described above has been supported by preliminary laboratory experiments that showed lowered pH and enhanced chloride content (as well as increased grout porosity) at the grout-void interface of a model anchorage assembly [Powers, 2001]. Adverse galvanic coupling with the anchorage and severe active corrosion were documented for that region. The local corrosion rates were on the order of 10^2 $\mu A/cm^2$, sufficient to cause mechanical failure of at least some wires after short periods, e.g. 1 year. Fast corrosion failure of an experimental anchorage has been also reported elsewhere [Tabatabai, 1995]. These cases suggest that some of the damage in the affected bridges may have been already quite advanced early during the service life of the affected bridges.

The objective of this investigation is to evaluate the validity of the corrosion mechanism suggested above, leading to a predictive model of the corrosion rate of PT steel based on properties of the system that may be quantified by measurement. Such prediction could then be applied to the selection of optimal grout properties and construction methods to minimize deterioration in future construction, and to appropriate preventive rehabilitation of existing structures. This paper presents activities in progress to characterize grout properties important to macrocell corrosion strength, polarization behavior of PT steel, and development of a predictive model. Findings are presented on the electrical resistivity of presently available commercial grouts, cathodic polarization behavior of PT wire, and the initial formulation of a macrocell corrosion model.

EXPERIMENTAL

Grout Resistivity Measurements: Five commercial grouts (designated A-E) from the Florida Department of Transportation FDOT qualified product list [Harkins, 2002] and a Type 1 plain cement paste were evaluated. The commercial grouts are newly formulated products yielding virtually no bleed water under standard test conditions. Water/grout (and water/cement for the paste) ratios are given in Figure 3. Before mixing, both tap water and grout were at ~20 to 22°C. About 7-kg grout/paste and the correspondent amount of water were mechanically mixed with a stirring paddle at ~2500 rpm in a 5-gallon bucket per manufacturer's recommendations. Immediately after mixing, a flow fluidity test (Modified ASTM C939) was conducted to verify that an efflux time between 9s and 20s was achieved for commercial grouts. A wick-induced bleed water test per ASTM C940 was also conducted to measure the amount of water that accumulated on the top of a 1000 mL graduated cylinder. The grout was then cast into plastic cylinder molds usually 10.2 cm (4 inch) long and 5.1 cm (2 inch) diameter fitted with 4 metallic contacts spaced ~2.5 cm apart in a row along the side forming a Wenner array. Measurements of electrical resistance were performed periodically with a Nilsson® Model 400 soil resistivity meter and the resistivity was obtained by applying a correction factor [Morris, 1996]. The cylinders were kept sealed tight and evaporation loss was negligible as indicated by periodic weight measurements.

Cathodic Efficiency of PT Wire: Wires 0.5 cm diameter, ~15 cm long and in the as-received mill finish condition were removed from a fresh roll of 1.5 cm, 1.86 GPa (0.6 inch, 270 ksi) A416 PT strands and used to determine their cathodic polarization behavior. The electrolytes used were saturated $Ca(OH)_2$ solution (SCS), simulated pore solution (SPS) and commercial grout. The SCS was prepared by adding 2 g/l $Ca(OH)_2$ to distilled water resulting in pH~12.6. The SPS had 2 g/l $Ca(OH)_2$, 3.70 g/l NaOH, and 10.5 g/l KOH; pH~13.3. Both the cut end of wires in the electrolyte and the region across the electrolyte/air interface were covered with a 2-component epoxy to expose only the side surface and avoid waterline corrosion. An activated titanium rod (ATR) electrode [Li, 2001, Castro, 1996] calibrated against a saturated calomel electrode (SCE) before and after the tests was used as the reference

electrode, while a graphite rod was the counter electrode. All tests were performed at room temperature, 21±1°C, and under naturally aerated conditions.

EXPERIMENTAL FINDINGS

Electrical Resistivity: As shown in Figure 3, the change of resistivity with time (average of multiple specimens of each type) can be divided into four zones according to the slope in a log-log diagram. All the newly-cast grouts, although with different water to grout ratios (W/G), had a similar low resistivity value (~100 Ohm-cm) during the first 10 hours (Zone I), followed by a sharp increase to ~1000 Ohm-cm during the next 20 hours (Zone II). In Zone III (from 30 to 1000 hr), all the grout resistivities kept increasing, reflecting the continuing hydration process with corresponding self-desiccation and reduced connectivity of the pore network. In Zone IV, the resistivity of some of the grouts began to give signs of approaching a terminal value of ~10 KOhm-cm while resistivity kept increasing for other grouts. The electrical resistivity of the paste, with a water to cement ratio (W/C) of 0.45, was much lower than that of the commercial grouts (W/G 0.23 to 0.30) in Zones III and IV.

Only a very small (~<0.1%) amount of bleeding water was seen around the strand area for the commercial grouts A~D and only about 0.3% bleeding for grout E. In contrast, there was ~1.6% bleeding water for the paste specimen. Preliminary internal relative humidity (RH) measurement results parallel these trends, suggesting that extensive self-desiccation [Bentz, 2001] occurs with the commercial grouts. Based on these findings, grout resistivity values from 10^3 to 10^5 Ohm-cm were used as ranging input parameters in the model calculations.

Cathodic efficiency tests: Figure 4 shows an example of oxygen reduction characteristics on duplicate PT wires at two immersion times in SCS. Similar cathodic polarization curves were obtained at 1 and 2 months, indicating a steady state had been reached. From these curves, an idealized Tafel slope value of 100 mV/decade was abstracted, together with a nominal exchange current density of 10^{-5} μA/cm^2 at a nominal equilibrium potential of 160 mV (SCE). The corresponding cathodic polarization line approaches the average trend (away from the open circuit potential) of the curves in Figure 4. Comparable results were obtained for SCS, SPS and the hardened grout, indicating relatively small variation of cathodic efficiency within the pH range present. The polarization behavior observed is also comparable to that seen for plain steel in similar environments [Li, 2001].

MODELING

System Modeled: The system simulated in this preliminary effort was a simple grouted cylinder with an axially placed 19-strand bundle (see Figure 5). The complicating geometry issue of strand distribution in the polyethylene duct as in Figure 5(c) was not taken into consideration. It was simply assumed that only the outer surface of the strands bundle in Figure 5(c) was electrochemically significant. Thus, an effective diameter of this equivalent was calculated from the total nominal cross section area of 19 0.6″-post-tensioning strands. A small 2 cm-long segment on the top (corresponding to the region close to the anchorage plate and most likely affected by chloride contamination and decreased pH, see Introduction) was designated as the actively corroding portion, while the rest of the surface area of the strands was treated as passive with only the cathodic reaction taking place on it. The present model is only a first step to understand this multifaceted system. Other factors, such as coupling to the surrounding anchorage metal, strand distribution and non-uniform grout properties will be addressed in subsequent stages of this investigation.

Electrochemical reactions: In keeping with alkaline conditions, the only important cathodic reaction considered in this paper was oxygen reduction (Eq.1). The only anodic reaction at the active segment of the strand was iron dissolution that was subject only to activation polarization (Eq. 2).

$$O_2 + 2H_2O + 4e \rightarrow 4OH^- \tag{1}$$
$$Fe \rightarrow Fe^{2+} + 2e^- \tag{2}$$

An additional anodic reaction, passive dissolution, was assumed to take place at the passive steel surface at a rate ip independent of potential. The cathodic reaction was assumed to take place at every point of the strand surface, at a rate given by the Bulter-Volmer equation (with concentration-dependence) as follows.

$$i_c = i_{oc} \frac{C}{C_0} e^{(\phi_s - E_{oc})/\beta_c} \tag{3}$$

The anodic reaction at the active steel surface was described by:

$$i_a = i_{oa} e^{(E_{oa} - \phi_s)/\beta_a} \tag{4}$$

The subscripts, c and a, denote cathodic or anodic reaction respectively (also see Nomenclature). These equations were put together in terms of local current densities, with exchange current density i_0, Tafel slope β, and nominal equilibrium potential E_0. ϕ_s is the potential at a point in the electrolyte adjacent to the strand surface. The strand itself was considered as an equipotential surface because of its high conductivity. The sign convention of the potential values was consistent with those published in previous papers [Kranc, 1994, 1997, & 2001].

Governing Equations: For simplicity, the grout used in the system was treated here as a homogeneous medium, which had constant electrical conductivity, σ, and oxygen diffusivity, D. Therefore, the governing equations at steady state for the electrical potential and oxygen diffusion in the grout could be expressed as Laplace's equation:

$$\nabla^2 \phi = 0 \tag{5}$$
$$\nabla^2 C = 0 \tag{6}$$

Boundary conditions: Per Ohm's law, the normal gradient (radial *r* direction) of the potential in the grout at the strand surface is proportional to the sum of all the current densities, that is, the net current across the electrolyte must match the net rate of electrochemical reactions. For oxygen transport at the strand surface, the local net O_2 supply, formulated by Fick's first law, was made to match the amount consumed by the cathodic reaction. The boundary conditions at longitudinal z direction and radial r direction were listed below. A detailed explanation of this approach is given elsewhere [Kranc, 1997 & 2001].

$$\sigma \frac{\partial \phi}{\partial r} = \sum i = i_a + i_c \quad \text{(active surface)} \tag{7}$$

$$\sigma \frac{\partial \phi}{\partial r} = \sum i = i_c + i_p \quad \text{(passive surface)} \tag{8}$$

$$\frac{\partial C}{\partial r} = \frac{i_c}{4DF} \qquad \text{(active and passive surface)} \qquad (9)$$

Dimensionless Equations: The above governing equations and boundary conditions can be cast in dimensionless form with the following definitions:

Variables: $Z' = \dfrac{Z}{L}$, $r' = \dfrac{r}{R}$, $C' = \dfrac{C}{C_0}$, $\phi' = \dfrac{\phi - E_{corr}}{\beta_a}$

Input parameters: $K = \dfrac{L}{R}$, $\xi = \dfrac{4FDC_0}{Ri_{corr}}$, $\eta = \dfrac{\sigma\beta_a}{Ri_{corr}}$ (Wagner Number), $i_p' = \dfrac{i_p R}{\sigma\beta_a}$

$$\beta_a' = \frac{\beta_a}{\beta_a} = 1, \quad \beta_c' = \frac{\beta_a}{\beta_c}$$

Substitution of these definitions into the governing equations yields:

$$\frac{\partial^2 \phi'}{\partial Z'^2} + K^2 \frac{\partial^2 \phi'}{\partial r'^2} + K^2 \frac{1}{r'} \frac{\partial \phi'}{\partial r'} = 0 \qquad (5')$$

$$\frac{\partial^2 C'}{\partial Z'^2} + K^2 \frac{\partial^2 C'}{\partial r'^2} + K^2 \frac{1}{r'} \frac{\partial C'}{\partial r'} = 0 \qquad (6')$$

In terms of dimensionless variables, the boundary conditions on the steel surface become

$$\frac{d\phi'}{dr'} = \frac{1}{\eta} C' 10^{(\beta_c'\phi')} - i_p' \qquad (7')$$

$$\frac{d\phi'}{dr'} = \frac{1}{\eta} C' 10^{(\beta_c'\phi')} - \frac{1}{\eta} 10^{(\beta_a'\phi')} \qquad (8')$$

$$\frac{dC'}{dr'} = \frac{1}{\xi} C' 10^{(\beta_c'\phi')} \qquad (9')$$

In the calculation, a finite difference formulation on a matrix of 201 nodes on the axial direction and 16 nodes on the radial direction was used and non-uniform grid size was adopted to simulate a 3 m-long system. Typically over 5×10^5 iterations were conducted to approach convergence, which was evaluated by observing the difference between the total computed anodic and cathodic current of the system. The final difference between those currents was typically less than 2%.

Cases Modeled: In this preliminary study, two cases based on oxygen availability at steel surface were modeled as outlined below.

Case A series. Limited oxygen transport was assumed, that is, oxygen could only diffuse through from the top grout surface and (to a much lesser extent) the HDPE duct. This assumption simulated an ideal condition, in which there were no cracks on the plastic duct. Additionally, the interstices between the king wire (central wire of an individual strand) and surrounding wires or inner strands and outer strands were assumed to be blocked and hence oxygen could not diffuse through this pathway either. The oxygen concentration (expressed in terms of the concentration of oxygen present in the grout pore solution) at the air-grout and air-duct interfaces was chosen as a constant 3×10^{-7} moles/cm^3 [Kranc, 2001], which is representative of equilibrium with the atmosphere as it may happen at the anchorage if sealing is not complete. All diffusivity values were converted to correspond to the manner in which

oxygen concentration was expressed. Based on the oxygen diffusivity and solubility values in HDPE per literature references [Rharbi, 1999, Epacher, 2000], the diffusion coefficient of oxygen there, D_{HDPE}, was set as 10^{-7} cm^2/s which is 1/100 of a typical value of oxygen diffusivity in water (10^{-5} cm^2/s). Other parameters used in the calculations are listed in Table 1. The experimental anodic parameters for post-tensioning wires are not available at this early stage and will be determined later. In this paper, the anodic polarization parameters used in the model are representative of the range commonly assumed for steel in concrete [Naish, 1990, Kranc, 1997].

Case B series. An oxygen concentration representative of atmospheric equilibrium (3×10^{-7} moles/cm^3) was available at all locations throughout the grout. This presented the worst condition (severe HDPE duct splitting and essentially free air transport through the interstices among strands) for corrosion attack since cathodic reduction of oxygen was not concentration dependent anymore.

Modeling results: Figure 6 illustrates the resulting oxygen concentration along the strand surface for the 10^4 Ohm-cm resistivity calculations. Oxygen concentration drops greatly in the active region due to the high consumption of oxygen associated with high local corrosion rate. At points far enough away from the active region, the oxygen demand decreases dramatically and the small flux through the HDPE duct wall (or alternatively through any minor leaks) is sufficient to finally maintain the surface concentration close to the atmospheric value. As expected, the oxygen concentration at the steel surface at or near steel surface becomes much lower for the lower grout oxygen diffusivity values. As seen in Figure 7, the active and passive regions are distinctly separated due to the model assumptions which cause those regions to behave as a net anode and a net cathode respectively. Two opposite factors influence the anodic current density profile in the first 2 cm (the active region): 1) decreasing oxygen concentration in the case A series and 2) increased coupling between the active and passive region as distance from the origin increases. Therefore, for the case A series where diffusivity is finite, the magnitude of the anodic current density in the active region first decreases with depth and then increases closer to passive steel zone. For the case B series with unrestricted oxygen access, the anodic current density does not experience an initial decrease. These trends are reasonably as expected and suggest that the model, despite its simplicity, may provide useful insight for understanding the otherwise complex conditions in an actual grouted anchorage system.

Figure 8 shows how the computed average corrosion current density over the total active region surface area depends on grout resistivity and oxygen diffusivity. Under the present assumptions, the calculations indicated that oxygen access was a dominant factor and the results were least sensitive to grout conductivity. For any given diffusivity, varying resistivity over two orders of magnitude changed the current density by less than one order of magnitude (although at very high resistivity the availability of electrolyte could be a limiting factor not included in the present model assumptions). In contrast, for example at a resistivity value of 10^4 Ohm-cm, the average corrosion current density increased from 4 to 73 μA/cm^2 when increasing oxygen diffusivity from 10^{-5} to 10^{-3} cm^2/s. Unrestricted oxygen access yielded 159 μA/cm^2. The corresponding corrosion rates (by Faradaic conversion assuming formation of Fe^{++} ions) ranged from ~0.05 mm/y to ~2 mm/y.

Given a corrosion rate value, a rough indication of the time required for outright overload failure of PT wires could be made based on common construction practice by conservatively assuming that the terminal stress in post-tensioned strands is on the order of 70% of the ultimate tensile strength. Thus, the occurrence of the failure of strands is likely to take place before corrosion from one side reduces the local cross section by ~30% (~1.5 mm in depth for the wires considered here). As a consequence, once corrosion attack initiates, the first wire failure under the average corrosion rates in the above examples could take place between < 1 year and ~ 30 years depending on oxygen availability. If corrosion were to

be further localized as suggested by the results in Figure 7, or due to the development of small pits, failure could occur even earlier. These simplified model projections are in agreement with the range of times to failure observed in the field, as well as the observations made in one preliminary laboratory study [Powers, 2001].

The present simplified model findings suggest that oxygen transport is a key element in corrosion development of PT systems. Further modeling development will address other critical issues, notably galvanic coupling between the strands and the cast-iron anchor body which can be important based on initial experimental evidence [Powers, 2001]. Other factors, such as the effect of periodic water recharge (involving the electrolyte availability issue mentioned above), iron dissolution kinetics, and the geometric distribution of grout and strands need to be incorporated in the model as well. Findings will be presented as work in this project progresses.

CONCLUSIONS

1.   Grouts meeting present qualification criteria had electric resistivity that increased with time toward apparent terminal values near or above 10^4 Ohm-cm, suggesting that significant self-desiccation was taking place.

2.   Oxygen-reduction polarization parameters of high strength wires in alkaline solutions representing grout, and in hardened grout, did not depend strongly on pH and were comparable to those encountered on plain steel in similar environments.

3.   A simplified mathematical model of a corroding strand bundle was formulated, incorporating both polarization and oxygen transport behavior. This initial computational study indicated that oxygen availability is a key factor in determining corrosion severity. Grout resistivity was a secondary factor within the range of validity of the model assumptions. Predicted corrosion rates were in general agreement with field and laboratory observations. Issues for subsequent model development were identified.

ACKNOWLEDGMENTS

REFERENCES

Bentz, D.P., Hansen, K.H., and Geiker, M.R., "Shrinkage-Reducing Admixture and Early Age Desiccation in Cement Pastes and Mortars", Cement and Concrete Research, 31(7), 2001, p1075

Castro, P., Sagüés, A.A., Moreno, E.I., "Characterization of Activated Titanium Solid Reference Electrodes for Corrosion Testing of Steel in Concrete", Corrosion, 52(8), 1996, p609

Corven, J., "Mid Bay Bridge Post-Tensioning Evaluation", Final Report, Florida Department of Transportation, October, 2001 http://www11.myflorida.com/structures/posttensioning.htm

Epacher, E., Tolveth, J., Krohnke, C., Pukanszky, B., "Processing Stability of High Density Polyethylene: Effect of Adsorbed and Dissolved Oxygen", Polymer, 41, 2000, p8401

Florida Department Of Transportation, "Sunshine Skyway Bridge Post-Tensioned Tendons Investigation", Feb, 2002http://www11.myflorida.com/structures/posttensioning.htm

Harkins, P., "Product Evaluation and Qualified Products List J-Grout/Mortar" Florida Department of Transportation, Aug, 2002, http://www11.myflorida.com/specificationsoffice/product.htm

Ghorbanpoor, A., Madathanapalli, S.C., "Performance of Grouts for Post-Tensioned Bridge Structures", Report NO. FHWA-RD-92-095, National Technical Information Service, Springfield, VA, 1993

Kranc, S.C., and Sagüés, A.A., "Computation of Reinforcing Steel Corrosion Distribution in Concrete Marine Bridge Substructures", Corrosion, 50(1), 1994, p50

Kranc, S.C., and Sagüés, A.A., "Detailed Modeling of Corrosion Macrocells on Steel Reinforcing in Concrete," Corrosion Science, 43, 2001, p1355

Kranc, S.C., and Sagüés, A.A., "Modeling the Time-Dependent to External Polarization of a Corrosion Macrocell on Steel in Concrete", Journal of Electrochemical Society, 144(8), 1997, p2643

Li, L., Sagüés, A.A., "Chloride Corrosion Threshold of Reinforcing Steel in Alkaline Solutions-Open-Circuit Immersion Tests", Corrosion, 57, 2001, p19

Morris, W., Moreno, E.I., and Sagüés, A.A., "Practical Evaluation of Resistivity of Concrete in Test Cylinders Using a Wenner Array Probe", Cement and Concrete Research, 26(12), 1996, p1779

Moreno, E.I., Sagüés, A.A., "Carbonation-Induced Corrosion of Blended-Cement Concrete Mix Designs for Highway Structures", Paper No. 636, Corrosion/98, NACE International, Houston, 1998

Naish, C., Harker, A., and Carney, R., "Concrete Inspection: Interpretation of Potential and Resistivity Measurements", In Corrosion of Reinforcement in Concrete, C. Page, K. Treadaway, and P. Bamforth, Eds., Elsevier Applied Science, London-New York, 1990, p314

Powers, R.G., "Corrosion Evaluation of Post-tensioned Tendons on the Niles Channel Bridge", Florida Department of Transportation, Gainesville, FL, June, 1999

Powers, R.G., Sagüés, A.A., Virmani, Y.P., "Corrosion of Post-Tensioned Tendons in Florida Bridges", Florida Department of Transportation, Tallahassee, Florida, 2001

Rharbi, V., Yekta, A., and Winnik, M.A., "A Method for Measuring Oxygen Diffusion and Oxygen Permeation in Polymer Films Based on Fluorescence Quenching", Anal. Chem., 71, 1999, p5045

Sagüés, A.A., Kranc, S.C., and Hoehne, R.H., "Initial Development of Methods for Assessing Condition of Post-Tensioned Tendons of Segmental Bridges", May, 2000 http://www11.myflorida.com/research-center/Completed_Proj/Summary_SMO/FDOT_BC374.pdf

Tabatabai, H., Ciolko, A. T., and Dickson, T. J., "Implications of Test Results from Full-Scale Fatigue Tests of Stay Cables Composed of Seven-Wire Prestressing Strands," Proceedings of the Fourth International Bridge Engineering Conference, Vol. 1, August 28-30, 1995, p. 266.

NOMENCLATURE

ϕ potential at a point of the electrolyte (all the potentials are in the saturated calomel electrode SCE, but referred to the metal, which was assigned to Zero potential. Note that this convention is the reverse of that commonly used to represent experimental data.)

σ grout conductivity

ξ dimensionless group for oxygen reduction boundary condition

η dimensionless group (Wagner Number)

β_a activation Tafel constant for iron dissolution (mV/decade)

β_c activation Tafel constant for oxygen reaction (mV/decade)

C   effective oxygen concentration at any point in the concrete (mole/cm^3) (For the calculations, C was expressed in terms of the concentration of oxygen present in the grout pore solution, which was assumed to be in equilibrium with any surrounding gas.)

C_0 effective oxygen concentration at grout surface

d   thickness of HDPE wall

D   effective diffusion coefficient of oxygen in grout

D_{HDPE} effective diffusion coefficient of oxygen in HDPE duct

E_{0c} equilibrium potential for the cathodic reaction of oxygen

E_{oa} equilibrium potential for the anodic reaction of iron

F   Faraday's constant

i_a anodic current density for iron

i_{oa} exchange current density for the anodic reaction of iron

i_{oc} exchange current density for the cathodic reaction of oxygen on iron

ip   passive current density of iron dissolution

r   radial direction

R_0 radius of the high-density polyethylene duct

R_1 radius of the nominal strand

Z   longitudinal direction

Superscript

$'$ dimensionless definitions

TABLE 1
System Dimensions and Calculation Parameters (see Nomenclature)

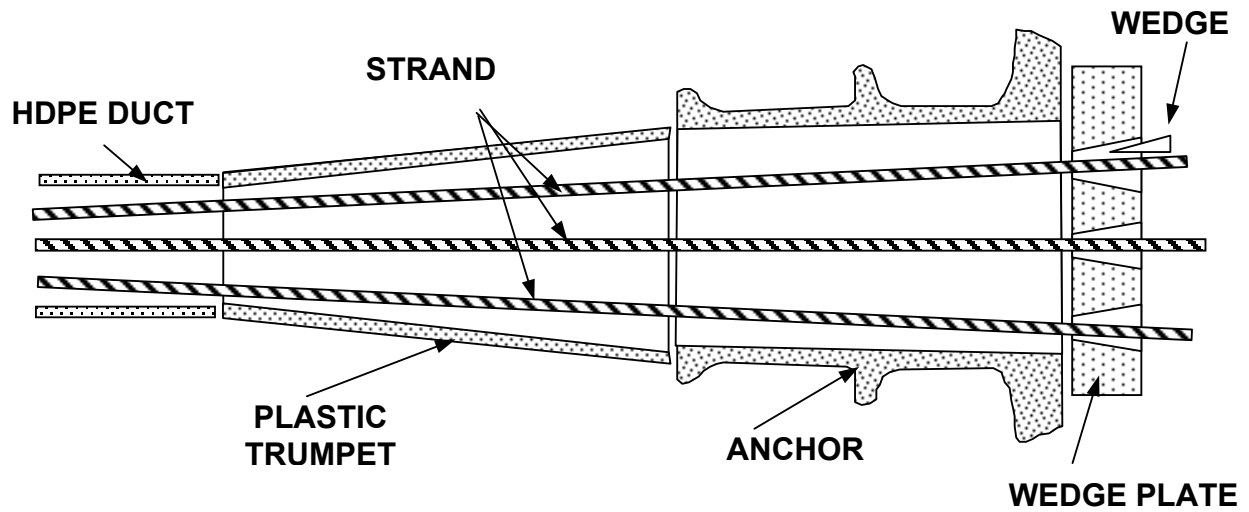| Parameter	Value	Parameter	Value
L (cm)	307.7	E_{oa} (mV vs SCE)	780
R_0 (cm)	5.08	E_{oc} (mV vs SCE)	-160
R_1 (cm)	3.32	ioa (A/cm2)	3×10^{-8}
C_0 (mol/cm^3)	3×10^{-7}	ioc (A/cm2)	1×10^{-11}
D (cm2/s)	0.001	βa (mV/decade)	60
σ (Ω-cm)$^{-1}$	0.00001~0.001	βc (mV/decade)	100
ρ(Ω-cm) (1/σ)	1000~100000	ip (A/cm^2)	10^{-8}
d (cm)	0.25		

FIGURE 1   Idealized Schematic of a Typical Anchorage System.
Only 3 Strands Shown for Clarity. Anchor, Wedge Plate
and Wedges are Ferrous Alloys

FIGURE 2 Severe Failure of Post-Tensioning Tendons near Cap Region (Corven, 2001)
a) Failed tendon at Niles Channel Bridge
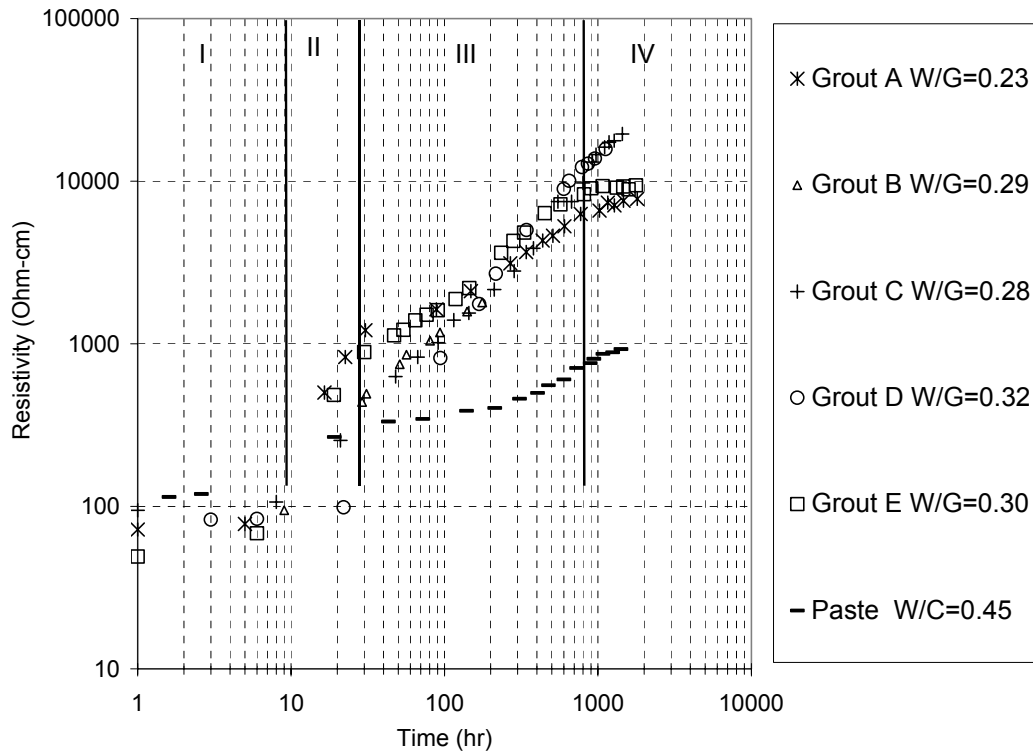b) Failed tendon at Column 133 NB of Sunshine Skyway Bridge

**FIGURE 3 Grout Resistivity as a Function of Time
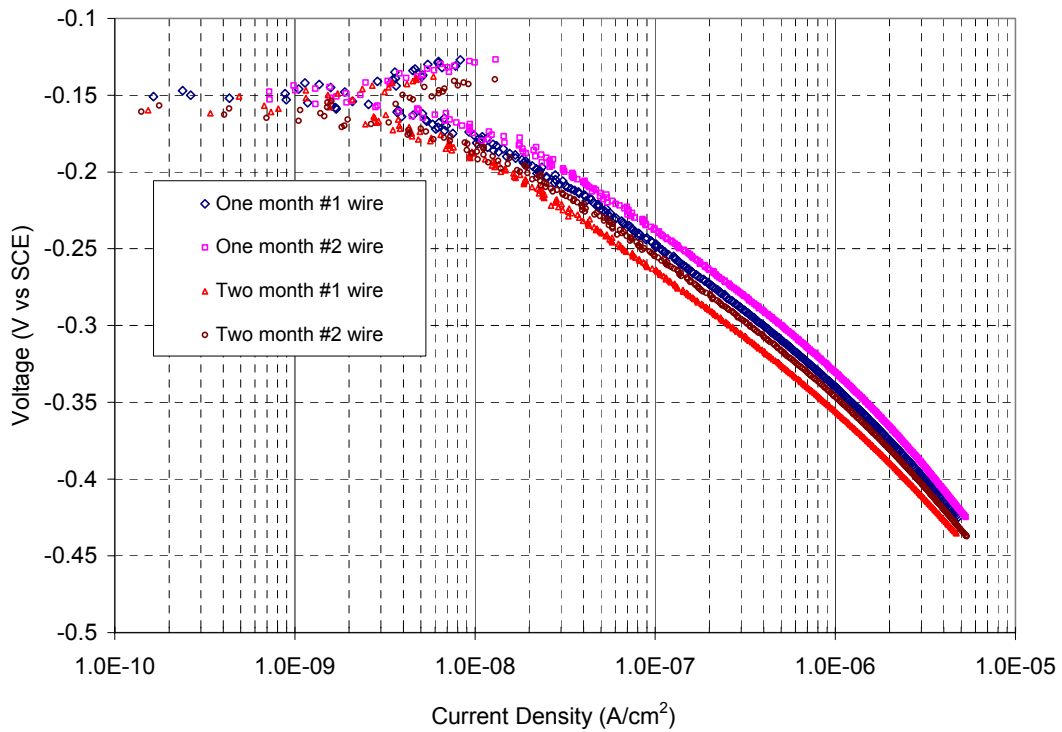(W/G: water to grout ratio; W/C: water to cement ratio)**

**FIGURE 4 Oxygen Reduction Polarization Curve of 0.2'' Post-Tensioning
Wire (SCS, scan rate=0.167 mV/s, open to air)**
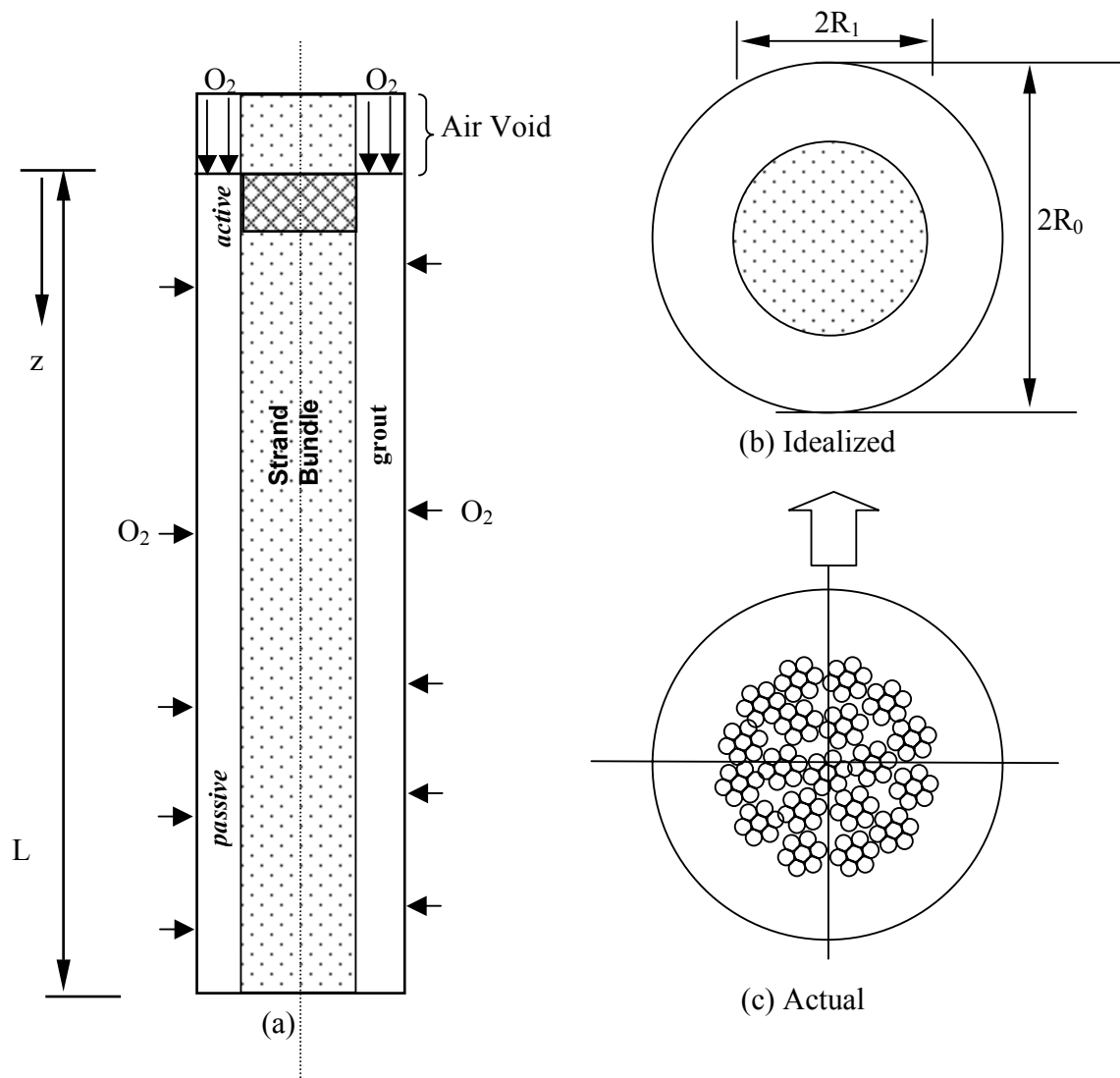
FIGURE 5 Schematic of a Simple Grout-Strand Cylinder System
(strands encased in HDPE duct)
(a)Longitudinal (b) Cross-section
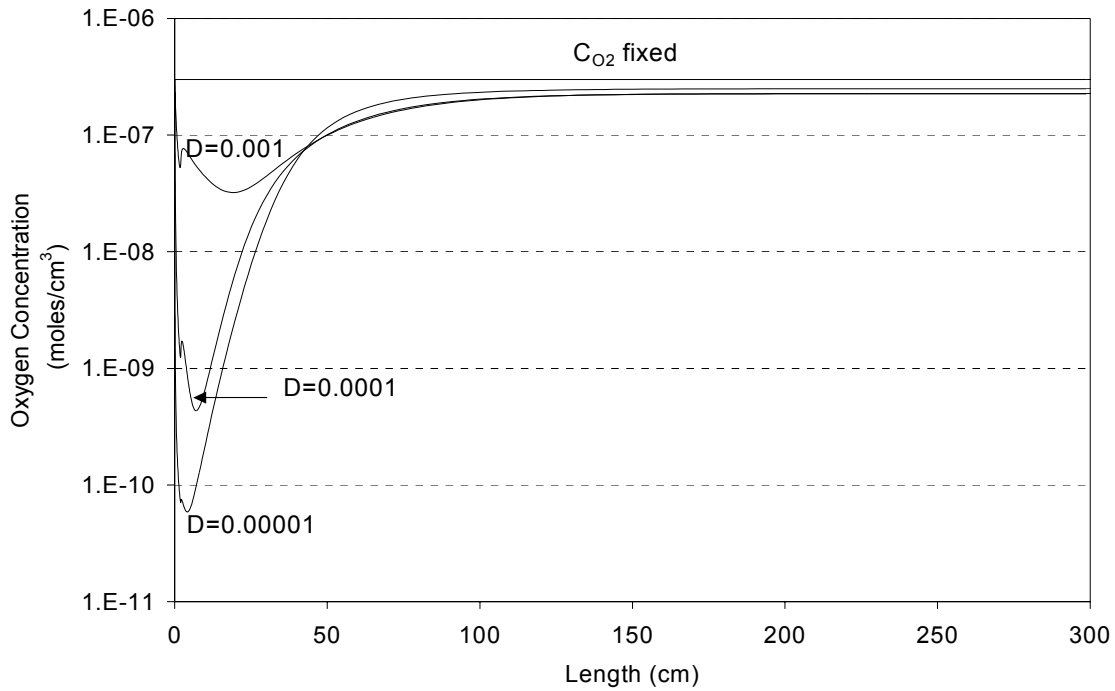**(c)19 7-wire strands in the HDPE duct, simplified to one nominal cylinder surface in a and b**

FIGURE 6 Longitudinal Distribution of Oxygen on the Grout Next to the Strand Surface (Resistivity=10^5 Ohm-cm). Values of oxygen diffusivity, D, for the case A series are in cm²/sec. C_{O2} is fixed for the case B series.
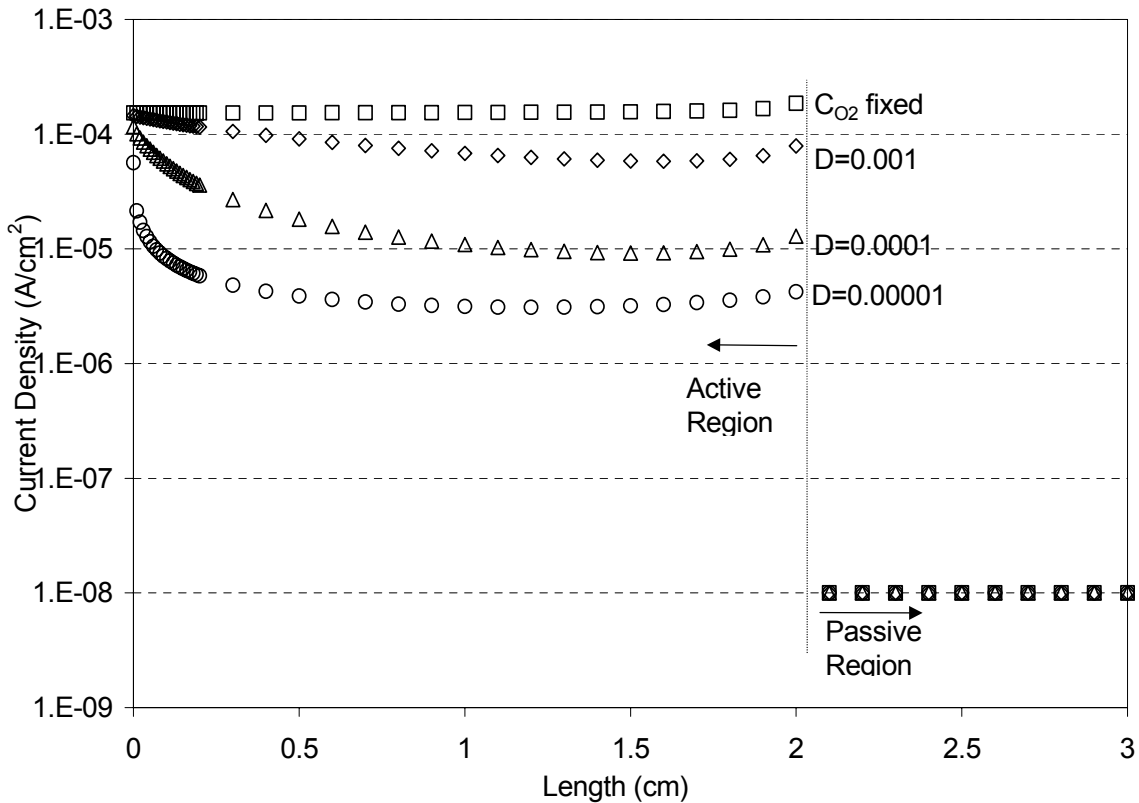

FIGURE 7 Longitudinal Distribution of Anodic Current Density (Region near active spot, Resistivity=10^5 Ohm-cm). Values of oxygen diffusivity, D, for the case A series are in cm²/sec. C_{O2} is fixed for the case B series.
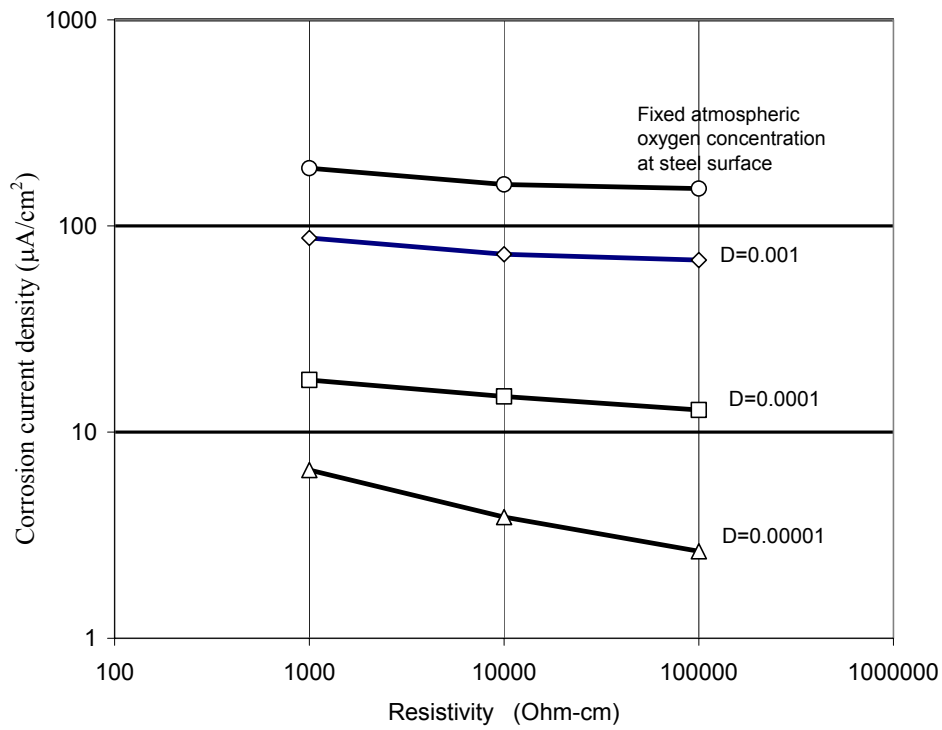
FIGURE 8 Average corrosion rate of the anodic zone as function of grout resistivity and oxygen diffusivity (Case A series), and for free oxygen transport to the steel surface (Case B series). Values of oxygen diffusivity, D, for the case A series are in cm^2/sec.